Published in final edited form as:
Magn Reson Med. 2006 October ; 56(4): 918–922. doi:10.1002/mrm.21013.

Exploring the Limits of RF Shimming for High-Field MRI of the Human Head

Weihua Mao, **Michael B. Smith**, and **Christopher M. Collins***
Center for NMR Research, Department of Radiology, The Pennsylvania State University College of Medicine, Hershey, Pennsylvania.

Abstract

Several methods have been proposed for overcoming the effects of radiofrequency (RF) magnetic field inhomogeneity in high-field MRI. Some of these methods rely at least in part on the ability to independently control magnitude and phase of different drives in either one multielement RF coil or in different RF coils in a transmit array. The adjustment of these drive magnitudes and phases alone to create uniform RF magnetic (B_1) fields has been called RF shimming, and has certain limits at every frequency as dictated by possible solutions to Maxwell's equations. Here we use numerical calculations to explore the limits of RF shimming in the human head. We found that a 16-element array can effectively shim a single slice at frequencies up to 600 MHz and the whole brain at up to 300 MHz, while an 80-element array can shim the whole brain at up to 600 MHz.

Keywords

MRI; high field; array; RF shimming; simulations

Recent hardware advances have been designed to facilitate unprecedented real-time control of the radiofrequency (RF) magnetic (B_1) field distribution with multiple variable voltage or current sources for MRI (1–6). This is a valuable development, in part because distinct current distributions in the coil or array used for excitation will likely be required to achieve homogeneous B_1 fields on different planes (7,8) or in different subjects (9) in human MRI at increasingly high field strengths. These hardware developments are also fueled in part by the expectation that multicoil tailored RF pulses (coordinating simultaneous application of specially-shaped RF and gradient pulses for spatially-selective excitation), such as those described as "transmit SENSE" (2) will be able to achieve volume-selective homogeneous excitation with shorter pulse durations than their single-coil counterparts (2,10,11). A few other multicoil approaches to achieving homogeneous images besides RF shimming and transmit SENSE, requiring differing amounts of foreknowledge of the RF field and varying degrees of pulse sequence manipulation, have also been proposed and discussed (12–14).

While many of these methods can theoretically produce more homogeneous excitations than RF shimming alone, they can require more foreknowledge of the field distributions (as for

*Correspondence to: Center for NMR Research, H066, 500 University Drive, Hershey, PA 17033. cmcollins@psu.edu.

designing tailored pulses), longer-duration RF excitations and higher SAR (as for adiabatic and composite pulses), and restrictions on sequence design beyond the excitation portion. Although RF shimming by itself shows much promise, it will also inevitably have limits. While Maxwell's equations may allow for existence of an almost perfectly homogeneous RF magnetic (B_1) field distribution on any one plane in an object as large as the human head at frequencies of hundreds of MHz, achieving this may require a large number of excitation sources. And achieving perfect homogeneity throughout an entire volume, even with a very large number of excitation coils, may not be possible due to the constraints of Maxwell's equations (7). Here we simulate a large number (16–80) of excitation coils using numerical calculations to examine the limits of B_1 field homogeneity that can be achieved by RF shimming alone on various single slices and over the whole brain volume at frequencies from 300 to 600 MHz.

MATERIALS AND METHODS

A 3D digital human head model was adapted from previous studies (15). It consisted of 23 different tissue types with a 5-mm isotropic resolution. Tissue electrical properties were assigned appropriately at each frequency of interest. Two elliptical, stripline coil arrays (16-element and 80-element) were modeled and driven at 300, 400, 500, and 600 MHz (see Fig. 1). The 16-element array geometry was based on designs from the University of Minnesota (5). Each of the arrays' elements was modeled as a 2 cm wide and 15 cm (for the 16-element array) or 2.5 cm (for the 80-element array) long, thin strip of copper, oriented in the longitudinal direction and placed with equal spacing on the surface of an ellipse with a short (left–right) axis of 21 cm and a long (anterior–posterior) axis of 24 cm. Both ends of each element were connected (with thin wires in a roughly radial direction) to a section of copper shield of corresponding length fitted to an elliptical shape with short and long axes of 23 and 27 cm modeled concentrically with the array. Longitudinal slots 5 to 10 mm wide were placed in the shield between each pair of neighboring elements, and 5 mm gaps between the ends of the elements also existed for the 80-element array. For the 16-element array, one current source was placed in each radially-oriented wire with sources at opposite ends of a given element having equal magnitudes and phases and being oriented in opposite directions. For the 80-element array, one current source was placed in the wire at the superior end of each element only. Tissue properties (conductivity and permittivity) were adjusted for each RF frequency (16).

The RF field driven by each element with a unit current was calculated with the finite-difference time-domain (FDTD) method using xFDTD software (REMCOM Corp., State College, PA). Then the results were loaded into in-house created C programs, and an optimization routine was used to vary the magnitudes and phases of the individual coils with the goal of improving RF homogeneity. Relative SD (SD divided by the average) was used to characterize homogeneity. The homogeneity of three different entities were optimized in separate procedures. The first is the flip angle, α

$$\alpha = \gamma\tau \left| \sum_{n=1}^{N} {}^{n}B_1^{+} \right| \quad [1]$$

where γ is the gyromagnetic ratio, τ is the pulse duration, N is the number of elements (16 or 80), and, ${}^{n}\mathrm{B}_1^+$ is the pertinent circularly-polarized vector component generated by the nth element.

The second entity optimized is the gradient echo signal intensity, $\mathrm{SI}_{\mathrm{GE}}$. Some methods of parallel reception serve to remove the receptivity distribution from the final image so that (ignoring anatomic features) $\mathrm{SI}_{\mathrm{GE}}$ is a function of the excitation distribution (17).

$$SI_{GE}=|sin\left(\gamma\tau|\sum_{\mathrm{n}=1}^{\mathrm{N}}{}^{\mathrm{n}}\mathrm{B}_1^+|\right)| \quad [2]$$

The third entity optimized is the spin echo signal intensity, $\mathrm{SI}_{\mathrm{SE}}$

$$SI_{SE}=|sin^3\left(\gamma\tau|\sum_{\mathrm{n}=1}^{\mathrm{N}}{}^{\mathrm{n}}\mathrm{B}_1^+|\right)| \quad [3]$$

Homogeneity was optimized over different region of interests (ROI). The whole brain including white matter, gray matter, and cerebral spinal fluid has 10,622 voxels. The single axial, sagittal, and coronal slices have 645, 541, and 461 voxels, respectively. A simple optimization algorithm was used to search for improved homogeneity of a single entity over an ROI by varying the current magnitude or phase in each element by a certain increment. If a more homogenous condition was found, this driving condition was taken. If no improvement could be found by changing any of the variables (current magnitudes or phases) by one increment, the increment was changed to −0.99 times its value and the process was repeated until no more improvements could be found and the increment was negligible in size. The initial increment was 100% of the current magnitude and 1 radian (about 57.3°) in-phase. All of the calculations were performed on a dual-processor workstation with 3.2 GHz central processing units (CPUs) and 2 GB of random access memory (RAM).

RESULTS

Figure 2 illustrates the effectiveness of RF shimming with the 16-element coil array at 300 MHz by showing the gradient echo signal intensity before and after optimization, where optimization was performed on each of three orthogonal slices and on the entire brain. Signal intensity on three orthogonal slices is presented for each optimal condition. In general, when the homogeneity is optimized on one slice, homogeneity is poor on orthogonal slices, but a very homogeneous distribution throughout all of the brain can be found using 16 elements at 300 MHz. With the optimal coil magnitudes and phases, the signal intensity distribution is very homogeneous and the variation in signal intensity can be reduced to less than 1% in single slices. Although the 16-element array can shim the field very well on single slices or throughout the whole brain at 300 MHz, it becomes less adequate at higher frequencies. Table 1 lists the relative standard deviation for different regions of interest at different frequencies. Figure 3 shows shimming effectiveness of the 16-element coil array at 600 MHz. The improvement from the original case is notable, but the final homogeneity is not nearly as good as at 300 MHz. Table 1 also indicates that

increasing the number of coils or reducing the ROI (selecting a single plane rather than whole-brain) can result in a significantly more homogeneous field after RF shimming. Figure 4 shows the shimming effects of the 80-element coil array at 600 MHz (14 T). The resulting homogeneity—even over the entire brain—is remarkably good at this high frequency when using 80 elements, though imperfections can be seen.

DISCUSSION

RF shimming, when coupled with parallel reception techniques, can produce very homogeneous MR images (17,18). RF shimming should be more effective at lower frequencies, with more elements, or over a smaller ROI. Here we investigate some of the limitations of RF shimming by going to very high frequencies (600 MHz) and using a large number of elements.

Very homogeneous images (with a relative SD of about 5% or lower) can be produced on a single plane with a 16-element array at 300 MHz, while the same array at the same frequency can produce fairly homogeneous images (with a relative SD of about 20% or lower) over the whole brain (Fig. 2). When the element number is increased to 80, the whole brain can be shimmed very well at 300 MHz, with a relative SD less than 1% on SI_{GE} for any ROI at 300 MHz (Table 1). At higher frequencies, the relative SD within the optimized whole brain increases. At a frequency as high as 600 MHz (14 T), a 16-element array can reach a relative SD less than 5% on SI_{GE} of a single slice (Table 1). At 600 MHz, an 80-element array can achieve a relative SD of less than 5% in the entire brain (Table 1). This indicates that with RF shimming alone very homogeneous excitations can be produced over the whole brain at very high frequencies if enough coils are used.

When an optimization is performed on a single plane, the resulting field on orthogonal planes becomes less homogeneous. The resulting variance in signal intensity on orthogonal planes is more exaggerated when optimization is performed on midsagittal or midcoronal planes (third and fourth rows of Figs. 2–4) than when optimization is performed on the midaxial plane (second row of Figs. 2–4). In all regions where there is rapid alternation between strong signal intensity and no signal intensity (closely-spaced black bands) the RF field strength is are high compared to that on the plane of optimization. This, coupled with inhomogeneity (strong field gradients), results in closely-spaced black bands as the flip angle passes through multiples of 180°, where the magnetization produces no signal. Similarly, the black regions within the brain seen on the midsagittal and midcoronal planes when the optimization is performed on the midaxial plane with 16 or 80 elements at 600 MHz (second row of Figs. 3 and 4) occur because regions of strong RF fields result in flip angles approaching 180° (17).

All of the optimization conditions are achieved by iteratively testing each parameter and comparing the nearest conditions, so that the optimal condition found may be a local optimum only. It is impossible to search all possibilities due to the large number of adjustable factors. For example, there are 160 variables (amplitudes and phases) to adjust for an 80-element system. Comparing just two possible conditions for each variable, the total number of possibilities is on the order of 10^{48}. Still, our optimization routine is extremely

simple, and a more sophisticated routine may yield better results. In addition, the element geometry and location can be improved. Still, the results in this study demonstrate the great potential of RF shimming alone at very high frequencies, even over the whole brain, when a large number of elements are used. Optimization time in this work depended on the number of elements, the ROI, the optimized entity, and the accuracy desired. The SI_{SE} took more calculation time than others. In the worst case, optimizing the 80-element system on the spin echo signal intensity of the whole brain at 600 MHz required about 26 min to reach an increment size less than 1% of that of the initial increment. Single-slice optimization, however, took less than 30 sec to reach the 1% increment size. Even less time was required for other optimized entities or fewer array elements. More sophisticated optimization routines may also achieve adequate results in a shorter amount of time.

RF shimming might be applied in vivo in a number of ways. For example, after separately mapping the complex RF receptivity field of each coil in an array, the optimal drive combination could be calculated quickly offline using the principle of superposition. Alternatively, an automated iterative procedure could be developed to improve the homogeneity of rapidly-acquired, low-resolution, low-contrast images by varying current magnitudes and phases without first mapping the fields.

In conclusion, RF shimming becomes more effective with a larger number of elements or smaller ROI. A 16-element array may be adequate for shimming a single slice at a high frequency up to 600 MHz, but more elements are needed to shim the whole brain to a similar degree at such a high frequency. When an adequate number of elements is available, RF shimming alone (without more complex approaches) may provide adequately homogeneous excitation in many cases for high field MRI.

Acknowledgments

Grant sponsor: National Institutes of Health (NIH), National Institute of Biomedical Imaging and Bioengineering (NIBIB); Grant number: R01 EB000454.

REFERENCES

1. Zhu, Y.; Watkins, R.; Giaquinto, R.; Hardy, C.; Kenwood, G.; Mathias, S.; Valent, T.; Denzin, M.; Hopkins, J.; Peterson, W.; Mock, B. Parallel excitation on an eight transmit-channel MRI system. Proceedings of the 13th Annual Meeting of the ISMRM; Miami Beach, FL, USA. 2005. p. 14
2. Ullmann, P.; Junge, S.; Wick, M.; Ruhm, W.; Hennig, J. Experimental verification of transmit SENSE with simultaneous RF-transmission on multiple channels. Proceedings of the 13th Annual Meeting of the ISMRM; Miami Beach, FL, USA. 2005. p. 15
3. Kurpad, KN.; Boskamp, EB.; Wright, SM. A parallel transmit volume coil with independent control of currents on the array elements. Proceedings of the 13th Annual Meeting of the ISMRM; Miami Beach, FL, USA. 2005. p. 16
4. Hoult DI, Kolansky G, Kripiakevich D, King SB. The NMR multi-transmit phased array: a Cartesian feedback approach. J Magn Reson. 2004; 171:64–70. [PubMed: 15504683]
5. Adriany G, Van de Moortele PF, Wiesinger F, Moeller S, Strupp JP, Andersen P, Snyder C, Zhang X, Chen W, Pruessmann KP, Boesiger P, Vaughan T, Ugurbil K. Transmit and receive transmission line arrays for 7 Tesla parallel imaging. Magn Reson Med. 2005; 53:434–445. [PubMed: 15678527]
6. Vaughan, JT.; DelaBarre, L.; Snyder, C.; Adriany, G.; Collins, CM.; Van de Moortele, P-F.; Moeller, S.; Ritter, J.; Strupp, J.; Andersen, P.; Tian, J.; Smith, MB.; Ugurbil, K. RF image

optimization at 7T and 9.4T. Proceedings of the 13th Annual Meeting of the ISMRM; Miami Beach, FL, USA. 2005. p. 953

7. Hoult DI. Sensitivity and power deposition in a high-field imaging experiment. J Magn Reson Imaging. 2000; 12:46–67. [PubMed: 10931564]
8. Ibrahim, T.; Patha, A. Homogeneous distributions of RF Fields over the human head volume at 7 Tesla. Proceedings of the 13th Annual Meeting of the ISMRM; Miami Beach, FL, USA. 2005. p. 2749
9. Collins, CM.; Swift, BJ.; Liu, W.; Vaughan, JT.; Ugurbil, K.; Smith, MB. Optimal multiple-element driving configuration depends on head geometry, placement, and volume of interest. Proceedings of the 12th Annual Meeting of ISMRM; Kyoto, Japan. 2004. p. 1566
10. Ulloa, JL.; Irarrazaval, P.; Hajnal, JV. Exploring 3D RF shimming for slice selective imaging. Proceedings of the 13th Annual Meeting of the ISMRM; Miami Beach, FL, USA. 2005. p. 21
11. Saekho S, Boada FE, Noll DC, Stenger VA. Small tip angle 3D tailored radiofrequency slab-select pulse for reduced *B*1 inhomogeneity at 3 T. Magn Reson Med. 2005; 53:479–484. [PubMed: 15678525]
12. Ledden, P.; Cheng, Y. Improved excitation homogeneity at high frequencies with RF pulses of time varying spatial characteristics. Proceedings of the 12th Annual Meeting of ISMRM; Kyoto, Japan. 2004. p. 38
13. Collins, CM.; Beck, BL.; Fitzsimmons, JR.; Blackband, SJ.; Smith, MB. Strengths and limitations of pulsing coils in an array sequentially to avoid RF interference in high field MRI. Proceedings of the 13th Annual Meeting of the ISMRM; Miami Beach, FL, USA. 2005. p. 816
14. Magill, AW.; Wilton, B.; Jones, A.; McKirdy, D.; Glover, P. A multiple element probe and sequential pulse sequence for ultra high field imaging—an improvement in B1 homogeneity. Proceedings of the 13th Annual Meeting of the ISMRM; Miami Beach, FL, USA. 2005. p. 815
15. Collins CM, Smith MB. Signal-to-noise ratio and absorbed power as functions of main magnetic field strength and definition of “90°” RF pulse for the head in the birdcage coil. Magn Reson Med. 2001; 45:684–691. [PubMed: 11283997]
16. Gabriel, C. Report AL/OE-TR-1996-0037. Air Force Materiel Command; Brooks Air Force Base, TX: 1996. Compilation of the dielectric properties of body tissues at RF and microwave frequencies.
17. Collins CM, Liu W, Swift BJ, Smith MB. Combination of optimized transmit arrays and some parallel imaging reconstruction methods can yield homogeneous images at very high frequencies. Magn Reson Med. 2005; 54:1327–1332. [PubMed: 16270331]
18. Li BK, Liu F, Crozier S. Focused, eight-element transceive phased array coil for parallel magnetic resonance imaging of the chest—theoretical considerations. Magn Reson Med. 2005; 53:1251–1257. [PubMed: 15906277]

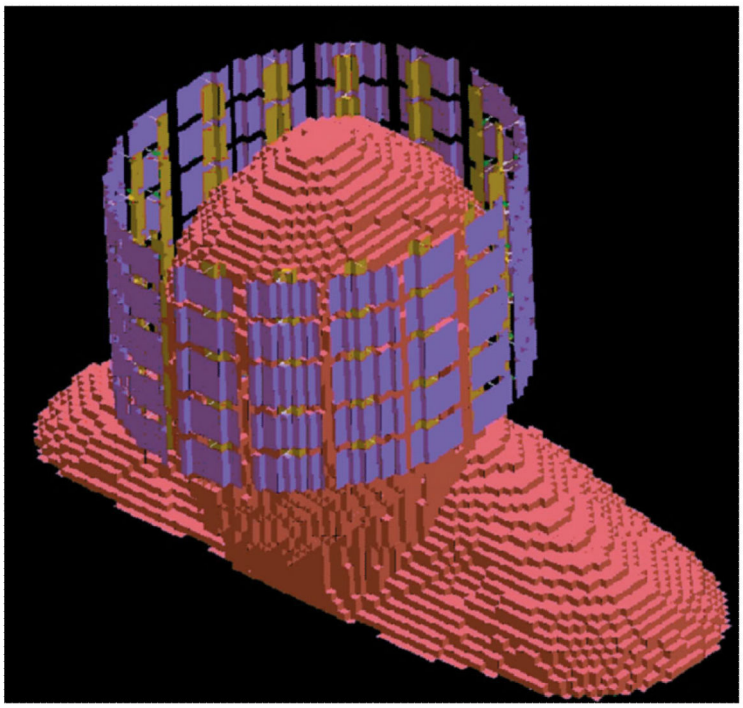

FIG. 1.
Shaded-surface rendition of the 3D digital head model and 80-element coil array.

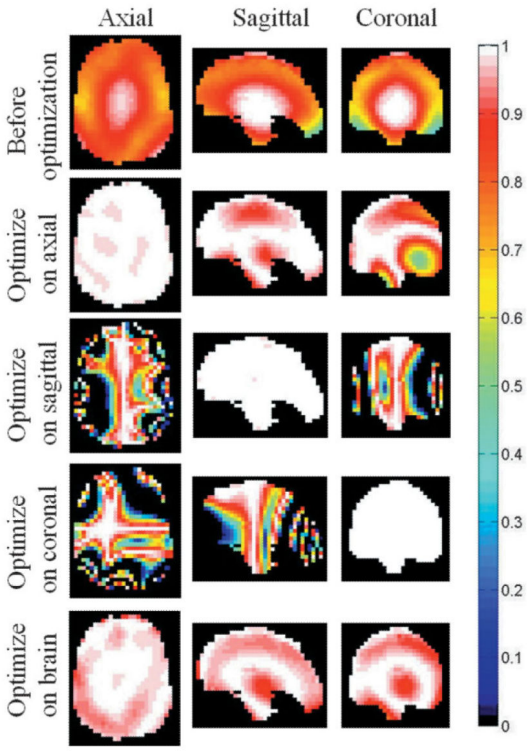

FIG. 2.

The 16-element optimization of gradient echo signal intensity maps of single slices and whole brain at 300 MHz. From top to bottom: standard drive before optimization, optimization on an axial slice, optimization on a sagittal slice, optimization on a coronal slice, optimization on the whole brain. Three orthogonal views (from left to right: axial slice, sagittal slice, and coronal slice) are shown for each driving condition.

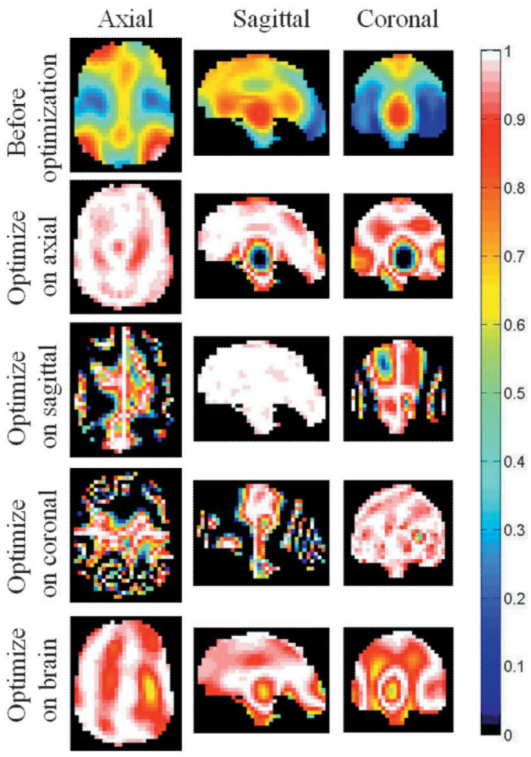

FIG. 3.

The 16-element optimization of gradient echo signal intensity maps of single slices and whole brain at 600 MHz. From top to bottom: standard drive before optimization, optimization on an axial slice, optimization on a sagittal slice, optimization on a coronal slice, optimization on the whole brain. Three orthogonal views (from left to right: axial slice, sagittal slice, and coronal slice) are shown for each driving condition.

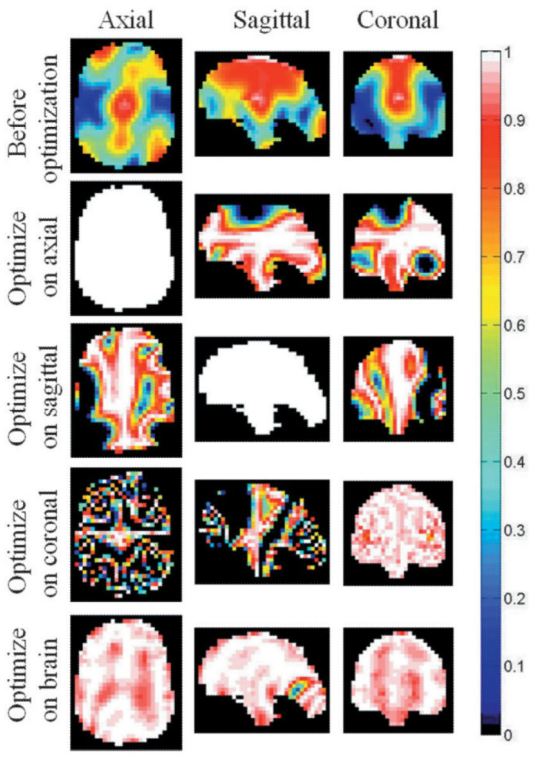

FIG 4.

The 80-element optimization of gradient echo signal intensity maps of single slices and whole brain at 600 MHz. From top to bottom: standard drive before optimization; optimization on an axial slice, optimization on a sagittal slice, optimization on a coronal slice, optimization on the whole brain. Three orthogonal views (from left to right: axial slice, sagittal slice, and coronal slice) are shown for each driving condition.

Table 1

Relative SD (RSD) for Optimization of Different Entities (Flip Angle α, SI_{GE}, and SI_{SE}) on Different ROIs at Different Frequencies With 16-Element and 80-Element Coil Arrays

		ROI		Optimize α		Optimize SI_{GE}		Optimize SI_{SE}	
Frequency (MHz)	Number of coils	Name	Number of voxels	RSD before shim	RSD after shim	RSD before shim	RSD after shim	RSD before shim	RSD after shim
300	16	Axial	645	0.138	0.060	0.096	0.0072	0.294	0.015
	80	Axial	645	0.203	0.006	0.195	0.0065	0.637	0.0003
	16	Sagittal	541	0.214	0.051	0.140	0.0037	0.400	0.015
	80	Sagittal	541	0.316	0.006	0.308	0.0001	0.673	0.0003
	16	Coronal	461	0.264	0.023	0.186	0.0012	0.520	0.004
	80	Coronal	461	0.330	0.059	0.321	0.0001	0.736	0.0003
	16	Brain	10226	0.202	0.156	0.146	0.0388	2.577	0.109
	80	Brain	10226	0.324	0.053	0.316	0.0046	0.786	0.018
400	80	Brain	10226	0.501	0.075	0.485	0.0094	1.098	0.032
500	80	Brain	10226	0.525	0.109	0.500	0.0181	1.199	0.054
600	16	Axial	645	0.370	0.122	0.263	0.0230	0.438	0.067
	80	Axial	645	0.467	0.012	0.451	0.0003	1.105	0.001
	16	Sagittal	541	0.304	0.055	0.196	0.0082	0.412	0.026
	80	Sagittal	541	0.405	0.009	0.381	0.0002	0.877	0.001
	16	Coronal	461	0.586	0.126	0.344	0.0559	0.742	0.097
	80	Coronal	461	0.675	0.019	0.649	0.0353	1.431	0.054
	16	Brain	10226	0.413	0.222	0.282	0.0979	1.066	0.213
	80	Brain	10226	0.512	0.124	0.490	0.0470	1.181	0.109